Hydrodynamic interaction between a pair of bubbles ascending in shear-thinning inelastic fluids

J. Rodrigo Vélez-Cordero[a], Diego Sámano[a], Pengtao Yue[b], James J. Feng[c], Roberto Zenit[a],*

[a] Instituto de Investigaciones en Materiales, Universidad Nacional Autónoma de México, Apdo. Postal 70-360, D.F. 04510, Mexico
[b] Department of Mathematics, Virginia Polytechnic Institute and State University, Blacksburg, VA 24061, USA
[c] Department of Chemical and Biological Engineering, University of British Columbia, Vancouver, BC, V6T 1Z3, Canada

ARTICLE INFO

ABSTRACT

The interaction of two bubbles rising in shear-thinning inelastic fluids was studied. The experimental results were complemented by numerical simulations conducted with the arbitrary Lagrangian–Eulerian technique. Different initial alignments of the bubble pair were considered. Similarities and differences with the Newtonian fluids were found. The most noticeable difference is the so-called drafting–kissing–tumbling (DKT) process: for the case of bubbles rising in thinning fluids, the tumbling phase does not occur and the pair tends to form a stable doublet. The DKT process is also influenced by the amount of inertia and deformability of the individual bubbles and the initial angle between them. The experimental and numerical results suggest that the thinning wake formed behind the bubbles plays an important role in the speed of the pair and the formation of clusters in thinning fluids.

1. Introduction

Bubble interactions have received considerable study in the literature owing to its inherent scientific interest and importance in applications such as gas–liquid contactors [1–3]. The study of two-bubble interaction was initially motivated by the coalescence phenomena due to its impact in bubble columns efficiency. That was how researchers took two different paths concerning this issue: one was the study of the coalescence mechanism itself, which is highly dependent on the liquid composition [4–6]; the other was the study of the trajectories that two bubbles take before coalescence [7–9]. In this work, the interaction of two bubbles ascending in shear-thinning inelastic fluids (non-coalescing conditions) is experimentally and numerically studied. First, we will make a review of the current literature of hydrodynamic interactions. In particular, to put our work in perspective, we focus on the Newtonian case.

For the case of creeping flow, Stimson and Jeffery [10] analytically predicted the velocity of two spheres moving in-line in terms of the separation distance between them. As widely described by [11], two bodies moving in this way in the creeping flow regime acquire a higher velocity than that attained by a single body; the velocity increases as the separation distance decreases. As the flow field does not have inertia, the bodies keep their distance without approaching each other. This trend is in agreement with experi-mental data [12] and with other analytical expressions [11], and applies as well to settling particles or rising bubbles.

When the inertia is small but finite ($Re \approx 0.25$) the vorticity around a spherical body looses its fore-aft symmetry and the trailing body acquires a higher velocity than the leading one, reaching the latter after some time. Crabtree and Bridgwater [7] were the first ones to approximate the trailing bubble velocity as the sum of the terminal velocity of the single bubble plus its wake velocity at the distance where the trailing bubble is found. This hypothesis was referred to as a 'superposition principle' by Bhaga and Weber [13]. In later works [13–15] this hypothesis was tested and confirmed for two in-line bubbles rising with Reynolds numbers up to O(100). Crabtree and Bridgwater also reported the curious phenomenon (not fully explained yet) in which the trailing bubble experiences a significant deformation (from oblate to prolate form) moments before touching the leading one. Such deformation was also reported and photographed by Narayanan et al. [14]. These last authors worked with different bubble sizes producing basically two different wake structures: one forming a thin trailing wake and the other forming a wake with a stable toroidal vortex. For the former it was observed that the Stimson and Jeffery's equation described well the rise velocities of the trailing bubbles even though it was formulated for creeping flows and spherical bodies. For the second case, a superposition principle similar to the one proposed by [7] was used. Bhaga and Weber [13] also worked with bubbles form-ing a wake with a toroidal vortex (Reynolds ≈ 80, Eötvös ≈ 70). The experimental measurements of the wake velocity were in agree-ment with the velocity calculated using the superposition principle. Manga and Stone [16,17] studied the effects of bubble deformability

---

* Corresponding author. Tel.: +52 55 5622 4593; fax: +52 55 5622 4602.
 E-mail address: zenit@unam.mx (R. Zenit).

in the interactions among them. They found that bubble alignment and coalescence is enhanced when the buoyancy forces are much larger than the restoring forces due to the interfacial tension on the bubble surface.

The interaction of two bubbles rising in potential flow was the subject of the theoretical work of van Wijngaarden and co-workers [18–20]. In these papers it was found that two bubbles rising in potential flow experience an attractive force if their angle of approach lies within ±54° from the horizontal, but feel a repulsion otherwise. The attractive force is due to the low pressure zone formed between the bubbles since the liquid velocity in this zone is larger. On the other hand, the repulsive force felt by the bubbles when they are aligned close to the vertical arrangement is due to the dynamic pressure that one bubble exerts on the other.

The behavior predicted in potential flows contrasts greatly with that observed in viscous dominated flows [21,12,22]. In such flows the behavior is actually the opposite: bubbles will experience a repulsive force if they lie near the horizontal alignment and an attraction if they lie close the vertical one. Such behavior can be explained in terms of the vorticity distribution: the vortices around each bubble will interact and repel each other if they are aligned in a horizontal orientation. This applies as well if a bubble rises near a vertical wall [21]. In the vertical alignment a net "suction" of the trailing bubble by the leading one occurs due to the vorticity asymmetry of the two bubble hemispheres. Now, it could happen that the two bubbles rising in this way will find an equilibrium distance between them when the viscous (attractive) and inertia (repulsive) forces cancel each other. That is to say, when the trailing bubble experiences the same amount of suction by the leading bubble wake and repulsion caused by its own upper wake when the two bubbles interact at short separation distances. This issue was in fact numerically analyzed by Yuan and Prosperetti [23]. They found such an equilibrium position between two in-line spherical bubbles rising in different hydrodynamic conditions ($20 < Re < 200$). Experimentally, an unstable equilibrium distance can indeed be found for clean bubbles which preserve its spherical shape as increasing the Re number (i.e., rising in silicone oils) [24]. Such equilibrium distance, which has been numerically found to be dependent on the Re number [23,25], is unstable in the sense that bubbles often escape from the vertical line.

Several experimental and numerical studies of the interaction of two bubbles at intermediate Re numbers have been devoted to the construction of the bridge that joins the creeping and potential flows [13,25–27,8,9]. These studies have revealed that two bubbles rising in-line follow the viscous dominated flow behavior at least up to a Reynolds number of O(1 0 0), i.e., the trailing bubble approximating the leading one. The question if an equilibrium distance appears or not during this process, i.e., the trailing bubble being ejected from the vertical line or reaching and making contact with the leading bubble, seems to depend on the shape and the surface properties of the bubbles. In particular, Kok [27] observed in contaminated water ($Re \approx 200$) that a trailing bubble reaches, touches, then turns its orientation angle to 0° with respect to the leading one and finally separates from it; a mechanism commonly referred to as the drafting–kissing–tumbling process [29]. This process is commonly observed in rigid bodies at low Re numbers [12,28]. In the case of two bubbles released side-by-side it has been found that they always repel each other for $Re < 30$ and attract each other for $Re > 200$, being the transition behavior dependent on the separation distance [22].

Regarding the drag force experienced by a pair of bubbles, in the vertical alignment the mean drag experienced by each bubble is less than the single bubble case. This is because the conjunction of the two bubbles will "form a body" aligned in the direction of the flow [23,30]. The prediction of the drag coefficients of two bubbles rising side-by-side is more complicated. With the help of the

experimental measurements of the drag coefficients in fixed rigid particles [31], together with the numerical works of [26,22], it has been found that two horizontal bubbles will experience less drag than the single one for low Reynolds flows ($Re < 50$). In this case the drag value increases, reaching the single bubble value, as the separation distance is increased. In small Re flows the long range interactions between bubbles start gaining importance; hence, two bodies moving side-by-side separated by a small distance, typically less than a bubble radius, will be surrounded by a unique vortex [31]; therefore, the two bubbles will find less resistance to motion. The opposite effect is found for high Re flows where wake instabilities can occur. This explanation is at least consistent with the behavior that has been observed in bubbly flows, that is, mild and strong bubble clustering in Newtonian and shear-thinning inelastic fluids at low Re, respectively, accompanied by an increase of the mean rise velocity with respect to the single bubble velocity [32,33]. On the contrary, a decrease of the mean bubble velocity with respect to the single one was observed as increasing the gas fraction (decreasing the separation distance between bubbles) in high Reynolds, low Weber flows [34].

These are some relevant studies of the hydrodynamic interaction of bubble pairs in Newtonian flows. One of the purposes of the present study is to determine the hydrodynamic interaction if non-Newtonian effects are considered. Important advances about this issue have been given by [35–39]. Using viscoelastic fluids, that is, fluids with shear-thinning and elastic behavior, Li et al. [35] and Radl et al. [36] elucidated that the viscosity gradients together with the amount of elasticity enhance bubble interactions. The corresponding decrease of the drag force was further related to the accumulation of residual stress via rheological simulations, a term coined by Li et al. [37]. In that work, the passage of bubbles was simulated by exerting consecutive shear rates to a fluid sample in a rheometer. The viscosity reduction in the bubble wake and the time lag needed for the zero-shear viscosity reestablishment extends the influence that a leading bubble has on other bubbles. This effect is not expected to occur in Newtonian fluids. The most outstanding behavior that has been observed regarding non-Newtonian effects was the repulsive effect that the formation of a negative wake produces between a leading Taylor bubble and a trailing one [38]. This effect has nevertheless been observed only in slug flow regimes where the bubbles fill completely the column diameter. Singh and Denn [40] and Tsamopoulos et al. [41] have numerically studied the rise of single bubbles and droplets in Bingham fluids. As these fluids have a yield stress value, the flow around the bubble is divided in three zones: an unyielded zone localized in the equatorial plane of the bubble, a yielded zone surrounding this one and which in turn is surrounded by a second external unyielded region. When the fluid properties and bubble size are such that the external and internal unyielded regions touch each other, the bubble will not move. Singh and Denn also studied the interaction of two and three bubbles rising in a Bingham fluid. During the collision, the shape evolution of the bubbles is similar to that seen in Newtonian fluids. The authors also noted that given a collection of fluid properties and bubble size that will result in the immobilization of one bubble, the addition of a second or a third bubble vertically aligned with the first one will produce enough stress to the fluid that the bubbles will start moving through the liquid.

The experimental and numerical studies cited above clearly demonstrate that when non-Newtonian effects are present (either elasticity or variable viscosity) the nature of hydrodynamic interactions is modified. The objective of the present work is to find the similarities and differences in the interaction of two bubbles (before and after collision) between Newtonian and shear-thinning inelastic fluids. It is well known that memory and thinning effects are two factors that are very difficult to untangle if are studied together, that is why we decided to start analyzing the effects of just one of them.
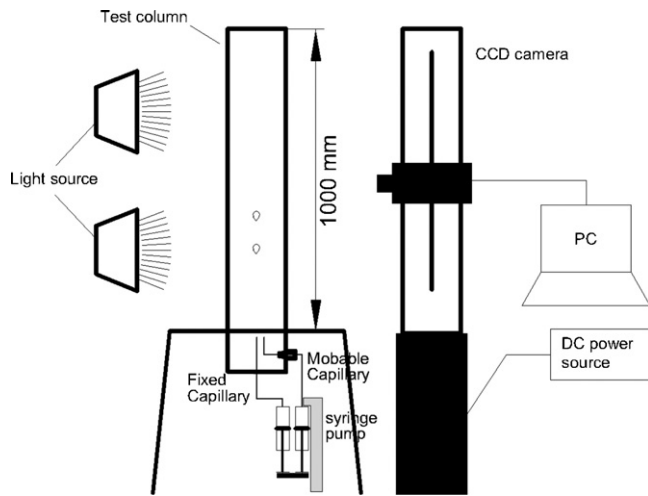
Fig. 1. Experimental setup.

Table 1
Bubble diameters obtained by the capillaries (I.D.: inner diameter of the capillaries).

	Capillary I.D.	Bubble diameter
Small	0.2 mm	2.1 mm
Medium	0.6 mm	2.8 mm
Large	1.2 mm	3.6 mm

2. Experimental setup

2.1. Column and bubble generation

The experiments were carried out with the setup shown in Fig. 1. It consists of a rectangular column made of transparent acrylic with an inner cross section of 5×10 cm^2. The column was filled with the test liquid up to a level of 100 cm measured from the base plate. Three capillary diameters were used to produce different bubble sizes. In order to avoid the generation of gas jets with variable volume, the hydraulic resistance through the capillaries has to be large. Hence, to generate individual bubbles, a capillary of 0.2 mm was inserted in the capillaries with the larger diameters, the latter being the ones that formed the bubbles. To generate in-line bubble pairs (vertical alignment), one capillary was inserted through the bottom of the column, using a sealed feedthrough (*Spectite Series PF*), at the center of the base plate. To generate bubble pairs aligned horizontally, a second capillary was inserted through the side wall, using an elbow and another feedthrough connector. In this manner the initial horizontal separation could be varied. Table 1 shows the bubble size that were obtained with capillaries having different inner diameters. Air was injected through the capillaries with a syringe pump (*KDScientific 100L*). To ensure that the polymer solution was completely at rest, a time interval of approximately 5 min was left in between experiments. Regarding this point, we did not observe a notable difference in the terminal velocities of two bubbles released one after the other for periods above one minute.
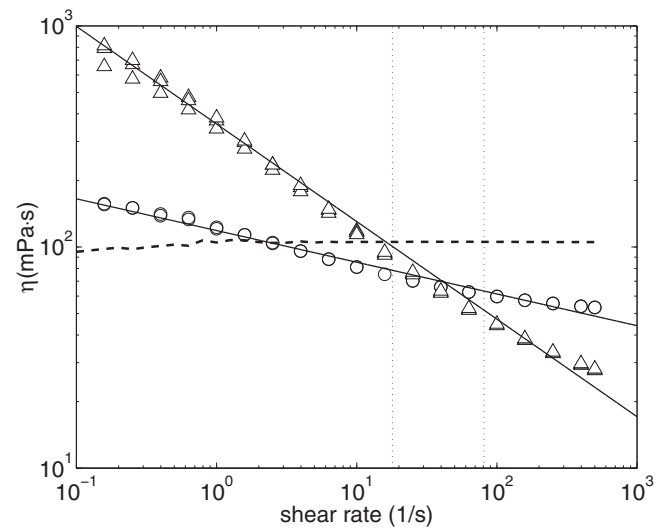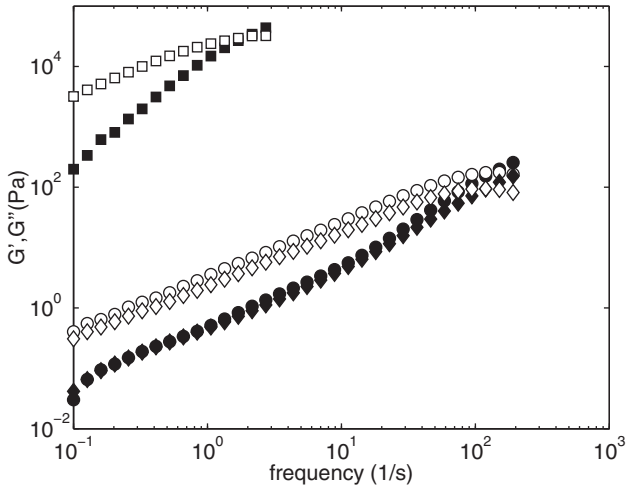

Fig. 2. Flow curves of the test fluids. η: apparent viscosity, (- - -) Newtonian fluid, (◯) $n = 0.85$, (△) $n = 0.55$. The vertical lines demarcate the shear rate range produced by the bubbles.

2.2. Fluids

We employed two shear-thinning fluids and a reference Newtonian solution. These fluids were also used in [33]. These shear-thinning fluids based on xanthan gum solutions follow a power law behavior with negligible elasticity in a wide range of characteristic flow times. As we are not interested in the coalescence mechanism itself, we also added 0.04 M of $MgSO_4$ to suppress it [4]. The details of the preparation of the solutions are given in [33]. The rheological measurements were conducted in a rheometer (*TA Instruments AR1000N*) with a cone-plate geometry (60 mm, 2°, a gap of 65 μm). The surface tension measurements were performed with a DuNouy ring (diameter of 19.4 mm, *KSV Sigma 70*). All the solutions were stirred before the surface tension measurement. The temperature of the room was 23 °C. The physical properties of the solutions are summarized in Table 2, the flow curves are shown in Fig. 2 and the oscillatory measurements in Fig. 3. Note that the frequency value (inverse of the relaxation time) at which the dynamic moduli curves intersect in the shear thinning (xanthan) solutions is about two orders of magnitude higher than the corresponding value of the viscoelastic (PAAm) reference solution. These measurements confirm that the relaxation time is comparatively smaller in the fluids used in this work, which indicate that elastic effects are negligible for our study.

2.3. Bubble size and velocity measurement

The bubble pairs were followed by a high speed camera (*MotionScope PCI 8000 s*) mounted on a vertical rail activated by a DC motor (Fig. 1). The velocity of the motor was regulated with a DC power supply. A recording rate of 60 frames/s was used. The image sequence obtained with the camera was binarized using a

Table 2
Physical properties of the fluids: ρ, density; σ, surface tension; η, viscosity; k, consistency index; n, flow index; $\dot{\gamma}$, shear rate range, estimated as $2U_{SI}/d_b$, achieved by the bubbles. U_{SI} and d_b are the terminal velocity and diameter of the single bubble, respectively. The percentages of liquid mixtures are given in volume terms, the percentages of the xanthan gum solutions in weight terms.

Fluids	ρ kg/m^3	σ mN/m	η or k mPa s^n	n	$0.4 < Re < 1.3$ s^{-1}
Newtonian: 83% glycerin/water	1214.6	61.9	104.2	1.0	34–72
0.02% Xanthan gum in 75% glycerin/water	1193.1	63.0	118.7	0.85	33–77
0.1% Xanthan gum in 60% glycerin/water	1152.1	65.0	360.0	0.55	18–81

Fig. 3. Dynamic moduli of the shear thinning solutions. Filled symbols: elastic moduli G', empty symbols: loss moduli G'', ($\bigcirc$) $n = 0.85$, ($\diamondsuit$) $n = 0.55$, ($\square$) a polyacrylamide (PAAm) reference solution (0.04% in 80/20 glycerin–water with 0.04 M MgSO$_4$). For the estimation of G' and G'' the procedure followed by [42] was used.

threshold value computed according to the Otsu's method provided by Matlab$^\copyright$. The equivalent bubble diameter d_b was calculated using the short and long diameters of the elliptic bubble projections:

$$d_b = (d_{MAX}^2 d_{MIN})^{1/3} \tag{1}$$

where d_{MAX} is the larger bubble diameter and d_{MIN} the shorter bubble diameter.

As the pictures were taken by a moving reference frame, we used a pattern of circles, glued on the side of the column, to calculate the displacement of the camera in between frames; once the displacement of the camera was known is was possible to compute the absolute displacement of the bubbles. This procedure consisted of two parts: first a pair of consecutive images (j and $j-1$) are selected from the sequence. Then the same circle of the reference pattern is identified in each image and the position of its centroid is calculated. After doing this, the reference position is taken from the first image; hence the location of the bubbles is determined and their evolution from one frame to the next one. This procedure is repeated for the entire image sequence. In this manner, the uncertainty in locating the bubble position is minimized eliminating problems due to vibration of the camera and changes in lighting. The velocity of the bubbles at the image j was calculated using a central difference scheme. The distance between bubbles was directly computed from the images.

3. Computational technique

The arbitrary Lagrangian–Eulerian (ALE) technique was used to numerically study the interaction of bubbles pairs with different angles of approach. This technique was developed by Hu et al. [43] to solve the motion of particles in two- and three-dimensional flows and modified by Yue et al. [44] to study bubble and foam problems in 2D and axisymmetric geometries. A detailed description of this technique and its algorithm can be found in [45,44]. The general features of the code will be described briefly.

The technique combines an Eulerian and Lagrangian descriptions of the flow and bubble motion using an unstructured finite element mesh. This means that the boundary nodes of the mesh follow the motion of the bubbles and the walls with possible slip. In the interior of the domain, however, the mesh motion does not follow the fluid flow but is computed from an elliptic partial differential equation which guarantees a smooth variation. The code

includes a remeshing tool that generates a new mesh upon detecting elements with unacceptable distortion. When this happens, a projection scheme is also invoked to project the flow field obtained on the old mesh onto the new one. The continuity and momentum equations were spatially discretized using the standard finite element Galerkin formalism and temporally discretized using the Crank–Nicolson scheme. The conservation equations are:

$$\nabla \cdot \mathbf{u} = 0 \tag{2}$$

$$\rho \left[\frac{\delta \mathbf{u}}{\delta t} + (\mathbf{u} - \mathbf{u_m}) \cdot \nabla \mathbf{u} \right] = -\nabla p + \nabla \cdot \eta [\nabla \mathbf{u} + (\nabla \mathbf{u})^{\mathbf{T}}] + \rho \mathbf{g} \tag{3}$$

where the viscosity is defined by the power-law model:

$$\eta = k \left[\sqrt{\frac{1}{2}(\dot{\gamma} : \dot{\gamma})} \right]^{n-1} \tag{4}$$

where $\mathbf{u}$ is the liquid velocity, ρ the density, p the pressure, η the viscosity, g the gravity, k the consistency index, n the flow index, $\dot{\gamma}$ the shear rate tensor and $\mathbf{u_m}$ the mesh velocity, which was obtained from the displacement of the mesh nodes according to the fixed computational coordinates. The referential time derivative $\partial/\partial t = \partial/\partial t|_{fixX}$ is made using the Lagrangian coordinate $\mathbf{X}$ affixed to the moving mesh.

The boundary conditions were the following: at the bottom wall the no slip condition was applied; at the right and left walls the slip condition in the y – direction was applied and the horizontal velocity component was set to zero; stress condition was applied at the liquid surface, both on the normal component ($\tau_{\mathbf{yy}} = p - p_0 = 0$) and the tangential component ($\tau_{\mathbf{xy}} = 0$); on the bubble surface the boundary condition was obtained from the Young–Laplace equation:

$$\mathbf{n} \cdot (-p\mathbf{I} + \tau) = (-p_b + K\sigma)\mathbf{n} \tag{5}$$

with the tangential components also set to zero (no surfactants). Here, $\mathbf{n}$ is the normal vector to the bubble surface, K the surface curvature, σ the surface tension and p_b the pressure inside the bubble. The initial pressure inside the bubble is given by $p_b = p_0 + \rho g(H - h) + 2\sigma/r$ where H is the height of the domain, h the height in which the bubble was released, r the half of the bubble diameter defined by Eq. (1) and p_0 the reference pressure (1.01×10^5 Pa). In the simulations, p_b is updated according to $p_b V_b = $ const, where V_b is the bubble volume.

The domain size was $16r \times 50r$. This size was the same for the 2D and axisymmetric calculations; therefore, $16r$ is the width for the 2D domain and also the diameter of the cylinder of the axisymmetric geometry; $50r$ is the height in both geometries. Nondimensionalized variables were introduced to the code considering the following scales: r for the length, r/U_{SI} for the time, U_{SI} for the velocity and ρU_{SI}^2 for the pressure and stress, U_{SI} being the terminal velocity of the single bubble. The viscosity, surface tension and gravity were non-dimensionalized using the experimental values of the Re ($\rho U_{SI} r/\eta$), We ($\rho U_{SI}^2 r/\sigma$) and Eo (Eq. (13)) numbers, respectively, and the scales mentioned above. The non-linear system equations are solved by Newton's method together with Krylov subspace iterative solvers such as the preconditioned generalized minimum residual (GMRES). The simulations were conducted in a computational grid located in Canada (glacier.westgrid or driftwood.iam.ubc). A typical job consisting of 25,000 elements takes less than a day to complete a run with 10,000 time steps. An upper limit for the time step is given by $\Delta t = 0.0005t^*$, where $t^* = r/U_{SI}$. For the single and in-line bubbles (Sections 4.1 and 4.2) we used the axisymmetric geometry while for the bubbles rising side-by-side or with other angles (Sections 4.3 and 4.4) we employed the 2D solver.
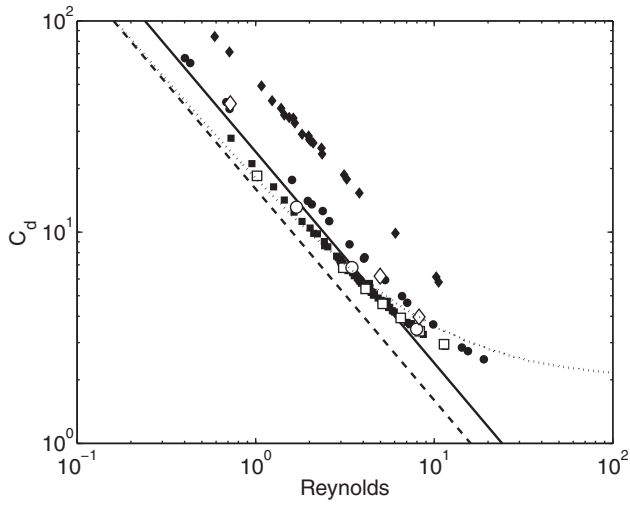
Fig. 4. Drag coefficient as a function of the Reynolds number for the single bubbles. Experimental values: (■) Newtonian fluid, (•) $n = 0.85$, (♦) $n = 0.55$. Numerical solutions: (□) Newtonian fluid, (○) $n = 0.85$, (◊) $n = 0.55$. (—) Stokes prediction, (– – –) Hadamard prediction, (. . .) Oseen correction for a fluid sphere $C_d = 16/Re + 2$.

4. Results

4.1. Single bubble results and benchmark simulations

The experimental drag coefficients for the single bubbles as a function of the Reynolds number are shown in Fig. 4. The numerical values are also included. The Reynolds number and drag coefficient C_d were defined as:

$$Re = \frac{\rho U_{SI} d_b}{\eta} \tag{6}$$

where

$$\eta = k\left(\frac{2U_{SI}}{d_b}\right)^{n-1} \tag{7}$$

and

$$C_d = \frac{4d_b g}{3U_{SI}^2} \tag{8}$$

We found that the Newtonian results lay between the Hadamard and Stokes drag predictions. Noticeable differences between the experimental and numerical results were just seen below a Reynolds number of one, where the numerical drag value approaches the Hadamard prediction while the experimental one the Stokes prediction. The thinning fluids values, on the other hand, lay above both theoretical solutions, meaning that the thinning condition results in larger drag than that for a Newtonian fluid at the same Re. Note that the agreement between the experimental and numerical values for the Newtonian fluid is good (square symbols in Fig. 4), indicating that the spatial resolution and the computational domain size were adequate. For the thinning cases, we found that the numerical terminal velocities were in all the cases higher (25% in the $n = 0.85$ fluid up to two times the experimental velocity in the $n = 0.55$ fluid) than those obtained in the experiments. The use of the Carreau model gave the same results. It is not clear if this difference is due to the choice of a definition of the apparent viscosity (Eq. (7)), or due to other effects such as the time that molecules take to attain a random orientation (zero-shear viscosity) after deformation or because there is an adsorption of the polymer molecules on the bubble surface thus changing the boundary conditions. In the following we will see that in spite of this inaccuracy of the numerical results, the essence of bubble pairing is still captured by the simulations.
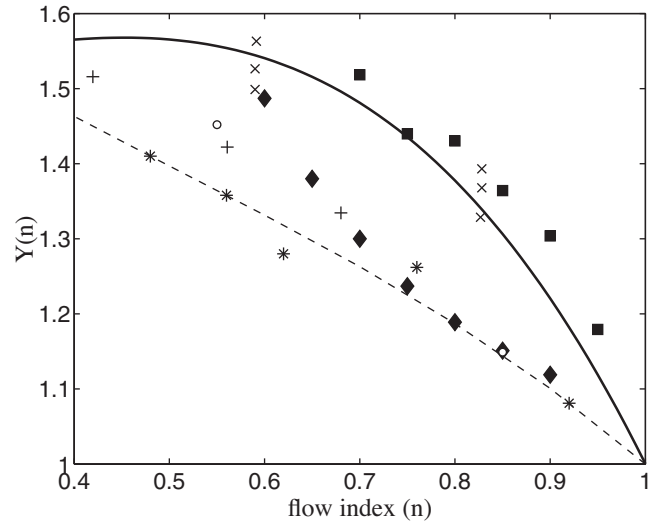
Fig. 5. Drag coefficient ratio $Y(n)$ as a function of the flow index. Numerical results: (■) $0.6 < Re < 1$, (♦) $7 < Re < 9$. Theoretical predictions: (—) Bhavaraju et al. [46], (– – –) Rodrigue et al. [48]. Experimental values: (○) this work $0.4 < Re < 1.2$, (×) 0.1 and 0.15% carbopol solutions from [46], (*) 0.1–2.0% CMC solutions, $Re < 6$ from [49], (+) 0.1–1.0% carbopol solutions with trietanolamyde, $Re = 3$ from [50].

In Fig. 5 the drag coefficient of the single bubbles rising in different shear-thinning liquids is presented in a different manner. The experimental and numerical drag coefficients were normalized by their Newtonian counterparts ($n = 1$) to form the ratio $Y(n)$:

$$Y(n) = \frac{Cd_{\text{thinning}}}{Cd_{\text{Newtonian}}} \tag{9}$$

The ratio $Y(n)$ has been used by several authors [46–48] to investigate the drag force in shear-thinning fluids. The theoretical values obtained by Rodrigue et al. [48] and Bhavaraju et al. [46] are shown in this figure as well as the experimental results obtained by other authors. The assumption of clean spherical bubbles was used in both theoretical studies for creeping flow; also both studies used a perturbation method. The only difference between them was the way of expanding the second invariant of the rate of deformation tensor γ. Following the standard notation for the drag coefficient used by [46–48], we calculated our experimental and numerical $Y(n)$ values for very low Re flows ($Re < 1$) using the Stokes and Hadamard solutions respectively:

$$Y(n)_{\text{exp}} = \frac{Cd_{\text{thinning}}}{Cd_{\text{Newtonian}}} = \frac{4d_b g/3U_{SI}^2}{24/Re} = \frac{d_b g Re}{18U_{SI}^2} \tag{10}$$

and

$$Y(n)_{\text{num}} = \frac{4d_b g/3U_{SI}^2}{16/Re} = \frac{d_b g Re}{12U_{SI}^2} \tag{11}$$

Theoretical, numerical and experimental results show the same trend: as the thinning behavior is increased (decreasing n) the bubbles experience more drag than their Newtonian counterparts. These observations can be interpreted as follows: the maximum shear rate experienced by the liquid is about U_{SI}/r, therefore the minimum viscosity value is approximately $k(U_{SI}/r)^{n-1}$ (note that for the drag estimation the equilibrium equation between buoyancy and drag forces was used and this expression do not need a viscosity value). For the single bubble case and at low Re numbers the shear rate decreases with the distance from the bubble, which in shear-thinning fluids result in higher viscosity values. The total effect is the increase of the resistance of the bubble motion, which can be seen by an increase of the pressure drag coefficient [51] which lessen the effect of the reduction of the friction drag

term that occurs as n decrease (this component of the total drag is actually negligible for bubbles without surface active agents).

We conducted other simulations with higher Reynolds numbers ($Re \sim 8$); the corresponding $Y(n)$ values are also shown in Fig. 5. In this case, since the Re number is not small the Hadamard prediction cannot be used and a direct comparison with the theoretical values [46–48] cannot be made. Therefore, to calculate the values of $Y(n)$ we divided the drag of the thinning fluid by the value attained by its Newtonian counterpart using the same physical parameters but changing the flow index value to one, leaving the same viscosity value at the characteristic shear rate U_{SI}/r. Other authors [52] have compared both cases, the Newtonian and thinning fluids, maintaining the same Reynolds number. Using this scheme, however, keeping the same physical data between fluids cannot be guaranteed. The $Y(n)$ values were thus calculated as:

$$Y(n) = \frac{Cd_{\text{thinning}}}{Cd_{\text{Newtonian}}} = \left(\frac{U_{SI_{\text{Newtonian}}}}{U_{SI_{\text{thinning}}}} \right)^2 \qquad (12)$$

The results have the same trend as in the low Re case, that is, the drag increases with the thinning behavior. Zhang et al. [53] made a similar comparison of their numerical terminal bubble velocities obtained with thinning and Newtonian fluids. In order to make the comparison they changed the value of the flow index (similar to what was done here) but considering a constant zero-shear viscosity value (we considered a shear-rate dependent viscosity). These authors found that the terminal velocity of bubbles rising in thinning fluids was higher than the corresponding Newtonian case.

4.2. Two-bubble interaction: vertical alignment

Let us first consider the numerical results. Initially we place two identical spherical bubbles one above another, with a center-to-center separation of $4r$ using the same physical properties as the ones used in the single bubble simulation with $Re \sim 8$. Upon start of the simulation, both rise and in time the lower bubble catches up with the upper one. When the bubbles reached a certain gap separation distance, two $Y(n)$ values (Eq. (12)) were calculated, one for the trailing bubble (comparing the bubble velocities of the Newtonian and thinning fluids) and another for the leading one. The results for two separation distances, $0.1r$ and $0.5r$, are shown in Fig. 6. In this figure we can observe that as the bubbles become closer to each other, the trend seen for single bubbles changes: the $Y(n)$ values fall slightly below one. This means that two bubbles rising one after the other in a thinning fluid experience less resistance than their Newtonian counterparts. This behavior is inherent to the way we made the thinning fluid simulations. As we previously said, we fixed the apparent viscosity corresponding to the characteristic shear rate U_{SI}/r of the single bubbles for both, the thinning and Newtonian cases. When for both is added a second bubble, the shear rate is increased in both fluids, the difference being that in the thinning case a zone with a lower viscosity near the bubbles will appear. The comparison made between the single bubble and bubble pair is similar to that made by [40], in the sense that the comparison depends on how the fluid properties are initially defined and serve as input information. For example, in this study single bubble and bubble pair simulations were done using the apparent viscosity calculated at the characteristic time of the single bubble as reference. However, this is an arbitrary numerical procedure since one can also define the reference viscosity for two bubbles (considered as a single one with the equivalent volume). The shear rate formed around a bubble or a pair of bubbles can be visualized using the numerical code. In Fig. 7 the shear rate fields are shown for the thinning fluid with $n = 0.5$ ($10 < Re < 16$). The shear rate attained around the bubble pair are clearly higher (up to four times) than that for the single bubble. As can be expected, the
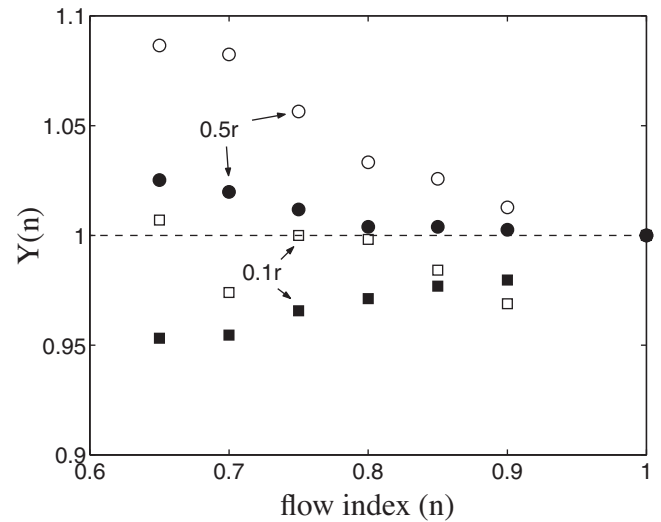

Fig. 6. Drag coefficient ratio $Y(n)$ as a function of the flow index for the in-line bubble pair; filled symbols: trailing bubble, empty symbols: leading bubble; ($\square$) gap separation distance of $0.1r$, ($\bigcirc$) gap separation distance of $0.5r$. As the bubble velocity was obtained from the average between the velocities at the top and bottom nodes of the bubble boundary, the minimum seen in the leading bubble for $0.1r$ could be due to bubble surface deformation.

zone with the higher shear rate surrounds the bubble pair, forming a single "jacket", when the bubbles become very close each other. Note that the numerical code is also capable to reproduce the axial elongation of the trailing bubble prior to contact. Also, the equilibrium position reported by [23] was not observed here for either the experimental or numerical tests.

The center-to-center separation distance between the bubbles as a function of the time is shown in Fig. 8 for the three bubble sizes used in this work. The experimental and numerical results are both shown using the dimensionless distance $d^* = \delta/r$ and the dimensionless time $t^* = t(U_{SI}/r)$, δ being the separation distance between bubble centers. In the following d_s^* is also used on several occasions and refers to an edge-to-edge or gap separation between bubbles. Three stages can be observed similar to the drafting–kissing–tumbling scenario reported for settling solid particles [12]. The first one
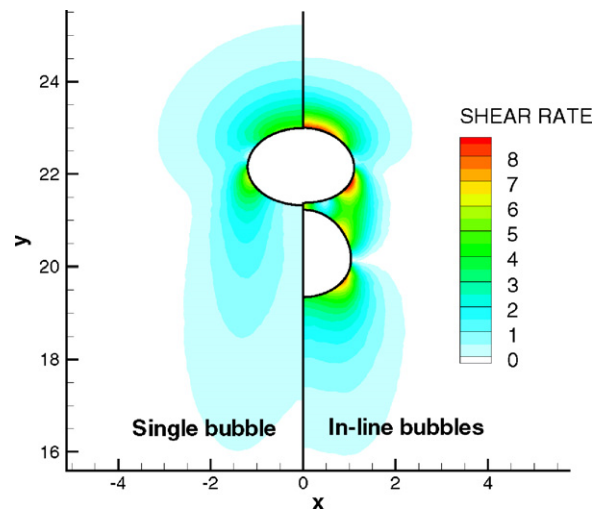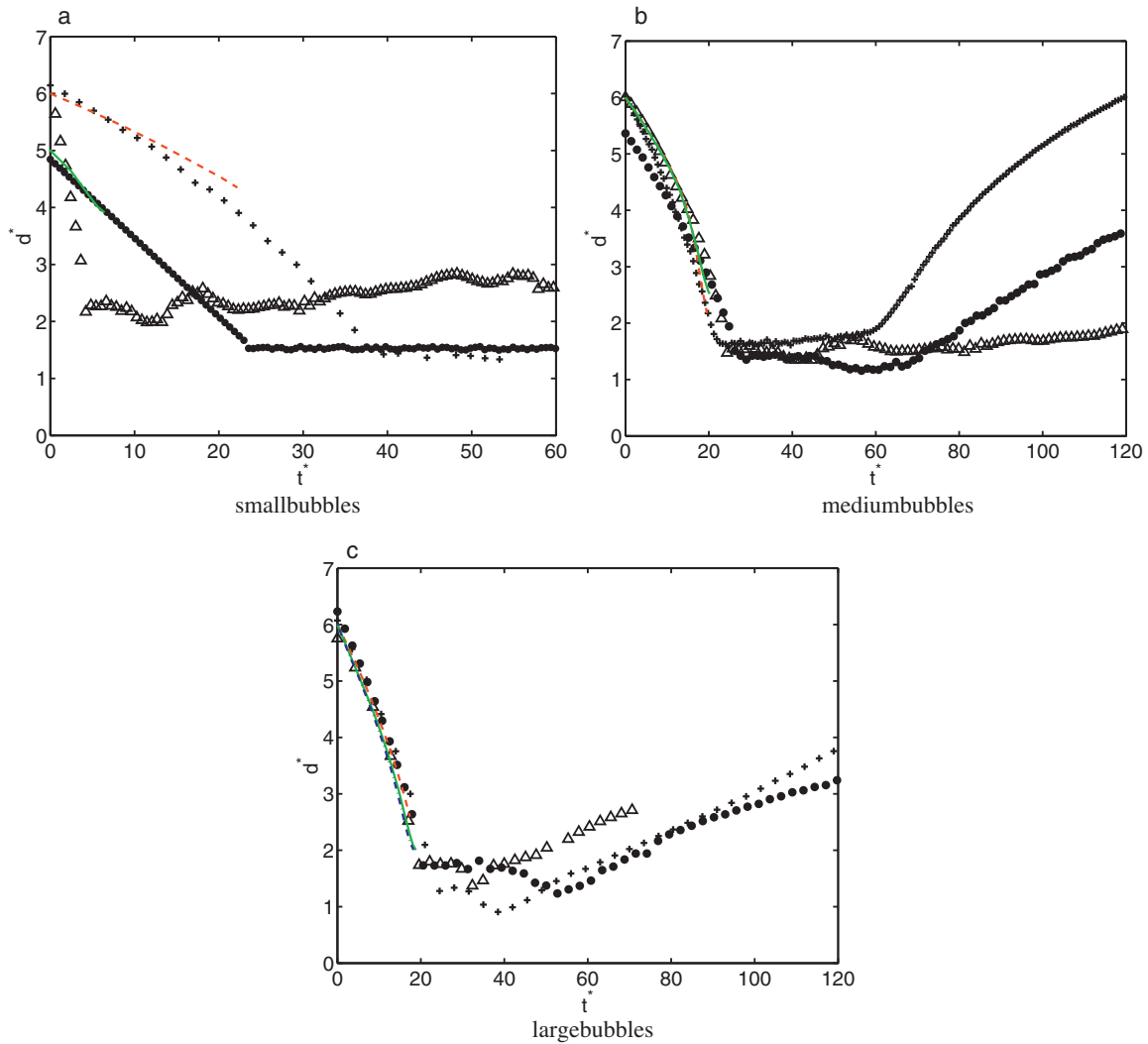

Fig. 7. Shear rate contours obtained for a single bubble and an in-line pair rising in the $n = 0.5$ fluid. The values were taken at the same time ($t^* = 5$) for both the single and bubble pair. The initial separation of the bubbles was $4r$. The shear rate was estimated using the formula inside the square brackets of Eq. (4) and normalized by the characteristic time r/U_{SI}.

Fig. 8. Center-to-center dimensionless distance as a function of the dimensionless time of two bubbles released in tandem. The initial separation distance was approximately $6r$. (a) $d_b = 2.1$ mm, $0.45 < Re < 4.5$, (b) $d_b = 2.8$ mm, $2 < Re < 6.4$, (c) $d_b = 3.6$ mm, $4.8 < Re < 13.1$. Experimental results: (+) Newtonian fluid; (●) $n = 0.85$ fluid; (△) $n = 0.55$ fluid. Numerical results: (dashed red line) Newtonian fluid; (continuous green line) $n = 0.85$ fluid; (dash-dotted blue line) $n = 0.55$ fluid (numerical results for this fluid using the smaller and medium bubble sizes are not shown due to the large computational time needed to complete the simulations). The computational domain size used for the Newtonian fluid with the smaller bubble ($Re \sim 1$) was $16r \times 70r$. (For interpretation of the references to color in this figure legend, the reader is referred to the web version of the article.)

(drafting) corresponds to the approaching of the trailing bubble towards the leading one. This stage is characterized by an almost constant negative slope of the $t^* - d^*$ curve, meaning that a constant approach velocity occurs. Note that when the Re number is increased (viscosity gradients become less important) the initial slope has the same value regardless of the value of the flow index (Fig. 8b and c). The numerical simulations for these early times t^* are in good agreement with the experimental results. The second stage (kissing) can be easily identified by the change of the initial slope. The contact of the bubbles is accompanied by an elongation of the trailing bubble followed by a slight contraction of both bubbles due to the collision. The third stage (tumbling or not-tumbling) is the one that marks the difference between Newtonian and non-Newtonian liquids. Concerning shear-thinning fluids, small and medium size bubbles ($d_b = 2.1$ mm and 2.8 mm) rising in the $n = 0.5$ fluid, and small bubbles rising in the $n = 0.85$ fluid, remained together after contact. The bubble pairs in these cases either maintained a vertical orientation (not-tumbling) or an orientation with a certain angle, switching their relative position as they ascended (Fig. 9b). In the rest of the cases the bubbles turned to the horizontal position after contact and separated (tumbling), as shown in Fig. 9a.
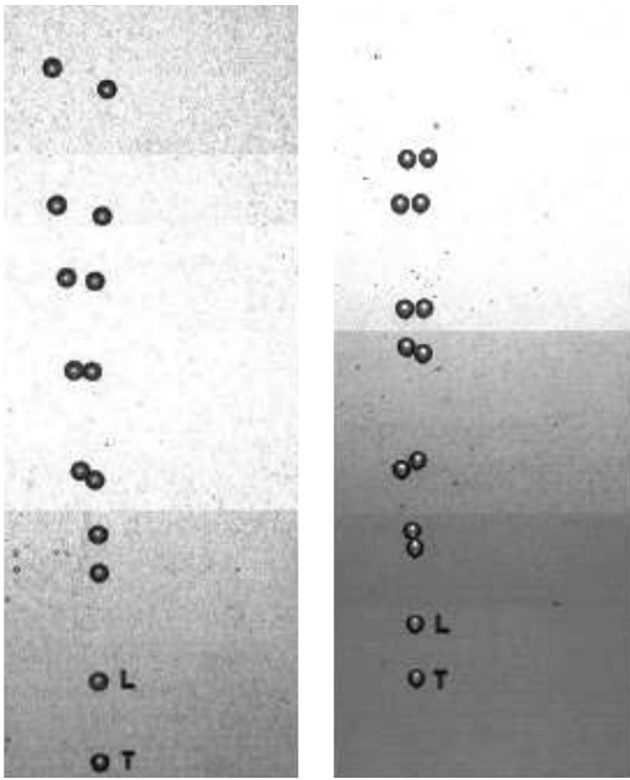
The condition to observe either free bubbles (the usual DKT process) or pair formation (missing the tumbling stage) after contact was mapped in an Eötvös–Reynolds plot considering the experimental single bubble data, as shown in Fig. 10. The Eo (also known as Bond) number is defined as:

$$Eo = \frac{\rho g d_b^2}{\sigma} \qquad (13)$$

This mapping was used to identify the regimes of free bubbles and clustering in bubbly flows [33]. As can be seen in the figure, the separation between cases corresponding to pair formation (filled triangles) and free bubble condition (empty triangles) is given approximately by $Mo = 10^{-3}$, which is the Morton number defined as:

$$Mo = \frac{g \eta^4}{\rho \sigma^3} \qquad (14)$$

This value was also found to be a critical number for the transition between free bubbles and clustering regime in bubble swarms rising in thinning fluids [33]. This suggests that the gas fraction has little effect on clustering break off in thinning fluids. Concerning
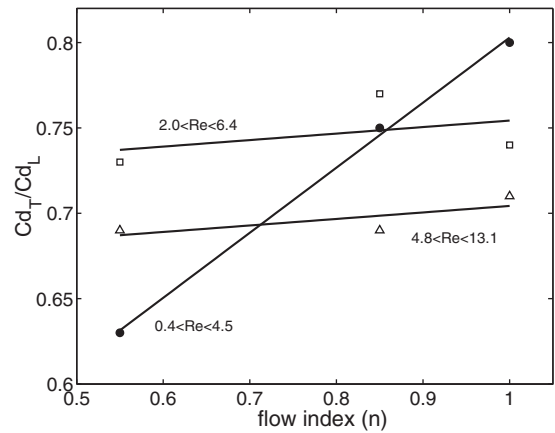
Fig. 11. Experimental drag ratio Cd_T/Cd_L in terms of the flow index n. (●) small bubbles, (□) medium bubbles, (△) large bubbles. Separation distance between bubbles: $\delta = 4r$.

In this work we found that two bubbles rising in tandem in the Newtonian fluid at low Re ($0.4 < Re < 1.3$) form a stable doublet (Fig. 8a). This contrast with the results obtained in [33] where for the same fluid and bubble size bubble pairing was not seen in bubbly flows. This indicates that bubble clustering in Newtonian fluids at low Re is greatly influenced by the amount of gas fraction [32], i.e., the Newtonian transition from free bubbles to clustering regime will be near the $Mo = 10^{-3}$ curve, but the transition can be different since it will also depend on the amount of gas fraction.

The fact that two bubbles rising in a Newtonian fluid can form a stable doublet supports the hypothesis that two *deformable* bodies moving in a fluid at low Re will prefer to move as a single body being surrounded by a common flow field. The deformability condition is emphasized since for rigid particles the pairing described here was not observed, even at low Re numbers [12]. This apparent contradiction supports, in fact, the general tendency found in [33]: for a given Eötvös number, bubbles tend to form clusters if the Re number is low; on the other hand, for a given Re, bubbles tend to form clusters if the Eo number is high (more deformable bubbles). This conclusion is not new: it was already reported by [16,17] for Newtonian fluids.
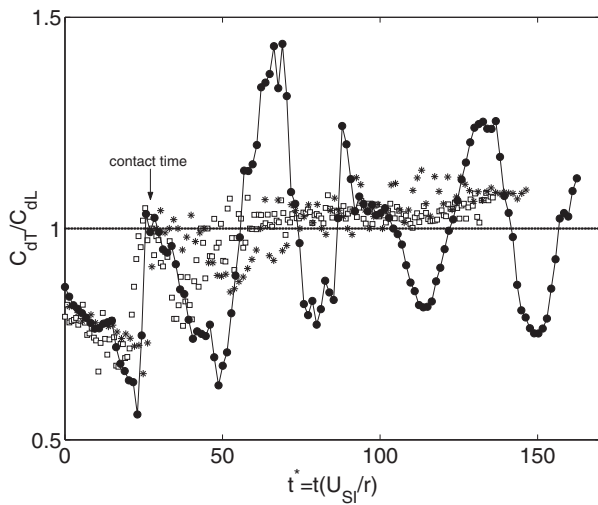
Fig. 8 suggests that the thinning effect during the drafting process can only be observed for low Re numbers, that is to say, when the rate of approach of the trailing bubble is dependent on the flow index (Fig. 8a). Using the experimental velocity of the bubbles, we can compute the ratio of the drag coefficient of the trailing bubble Cd_T to the leading one Cd_L as:

$$\frac{Cd_T}{Cd_L} = \left(\frac{U_L}{U_T}\right)^2 \qquad (15)$$

where U is the instantaneous velocity of the bubbles. The drag ratio at a separation distance of $\delta = 4r$ for different values of the flow index n is shown in Fig. 11. The data with $0.4 < Re < 4.5$ (small bubbles) confirms the observation that the mean drag of a bubble pair is less than its Newtonian counterpart, unlike the single bubble case. Such effect is nevertheless seen only at low Re values. As inertia is increased, the decrease of the drag with the flow index is more subtle.

In the tumbling stage, if it is observed, the drag ratio value becomes almost one. This can be seen in Fig. 12 with the Newtonian and $n = 0.8$ fluids. In this figure the experimental drag ratio Cd_T/Cd_L for the medium bubble size was plotted as a function of the dimensionless time. The values of the Newtonian fluid correspond to the case shown in Fig. 9a. For the case when the bubbles continued traveling as a pair (Fig. 9b, $n = 0.55$ fluid), the evolution of the drag ratio is very different (filled circles in Fig. 12). In this case,
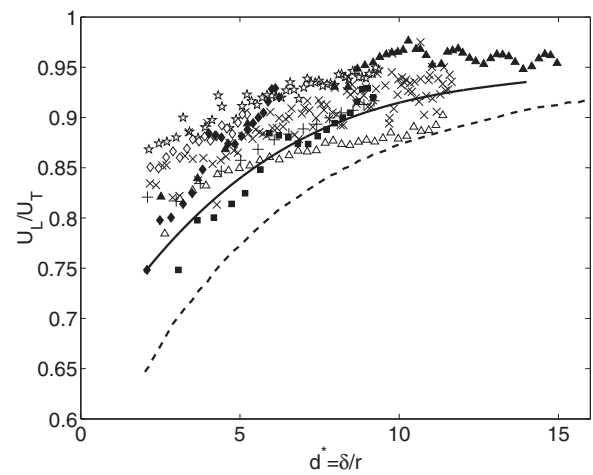

a   Newtonian, Eo=0.9, Re=1.3   b   n=0.55, Eo=0.7, Re=4.5

Fig. 9. Non consecutive snapshots of the bubbles position taken with the movable camera. The bubble size is 2.8 mm. The size of the image is approximately 7×17 cm^2. The Δt between shots is 0.5 s. (L) leading and (T) trailing bubbles. The indicated Re number corresponds to the maximum value reached by the bubbles.

Newtonian flows, in [32] it was found that clustering can also occur when long range interactions are significant (low Re numbers), but in that case the effect is rapidly hindered by the increase of the gas fraction.
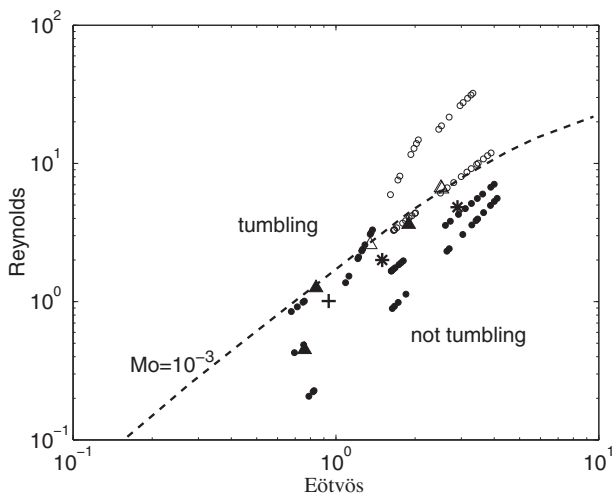
Fig. 10. Cluster condition formation mapped in a Eo–Re curve for the single bubbles. (▲) hydrodynamic conditions where the tumbling stage was not seen in the thinning fluids, (△) hydrodynamic conditions where the tumbling stage was seen in the thinning fluids, (− −) $Mo = 10^{-3}$, (*) free bubbles after contact in the Newtonian fluid, (+) pair formation after contact in the Newtonian fluid. The (●) and (○) symbols correspond to the cluster and free bubble conditions found in bubble swarms [33]. The iso-Morton line was taken from [54]. The Morton number in an Eo–Re plot increases from top to bottom.

Fig. 12. Experimental drag ratio Cd_T/Cd_L in terms of the dimensionless time t^*. (□) Newtonian fluid, (*) $n = 0.85$ fluid, (●) $n = 0.55$ fluid. The bubble diameter is $d_b = 2.8$ mm.

Fig. 13. Velocity ratio U_L/U_T in terms of the dimensionless distance d^*. (*) $d_b = 2.1$ mm, Newtonian fluid, (×) $d_b = 2.8$ mm, Newtonian fluid, (+) $d_b = 3.6$ mm, Newtonian fluid, (◇) $d_b = 2.8$ mm, $n = 0.85$ fluid, (△) $d_b = 3.6$ mm, $n = 0.85$ fluid, (■) $d_b = 2.1$ mm, $n = 0.55$ fluid, (◆) $d_b = 2.8$ mm, $n = 0.55$ fluid, (▲) $d_b = 3.6$ mm, $n = 0.55$ fluid. (− −) theoretical solution for rigid spheres [10], (—) theoretical solution for gas bubbles [56].

the movement of the bubbles forming the pair produces an oscillatory behavior of the drag ratio Cd_T/Cd_L: when the trailing bubble catches the leading one, the pair turns towards the horizontal alignment due to the pressure directed against the bubble motion. This horizontal arrange is nevertheless not stable because it leads to the separation of the bubbles [22], which in turn causes a passage form low to high viscosity zones since the characteristic shear rate is decreased. A possible configuration is then a diagonal alignment. The bubble located at the front will cause a reduced viscosity path, hence the bubble in the back will be accelerated, reaching the bubble at the front and passing it. The process is repeated again. A similar periodic movement has been observed for the case of groups of settling particles formed by three (experimental results, $Re < 0.2$) or four bodies (numerical results, $Re \ll 1$) [28,55,17]. However, the periodic movement observed here for the case of two bodies has not been observed in Newtonian fluids, neither for settling particles [12,28] nor for ascending bubbles (this work). A periodic transverse movement between a pair of bubbles rising side-by-side has been observed in Newtonian flows [9], but this occurs at $Re \sim 300$, which has very different hydrodynamics than those obtained at low Re. Hence, we believe that the oscillatory behavior seen in Fig. 12 is due to non-Newtonian effects.

Apart from the differences found during the tumbling stage, the drafting process observed in the different fluids is very similar, the most significant differences being those at low Re numbers. Fig. 13 shows the bubble velocity ratio U_L/U_T as a function of the separation d^* for all the fluids and bubble sizes. The plot includes all the data prior to bubble contact ($\delta > 2r$). In spite of the data scatter the trend is close to the analytical solution of Rushton and Davies for gas bubbles [56] rising in Newtonian fluids. This analytical solution was based on the theoretical study made by [57], which took into account the velocity of the leading wake. The agreement of the experimental data with the theoretical prediction suggest that the principle of superposition is also valid for shear-thinning fluids. The deviation of the experimental values from the theoretical prediction at short separation distances ($\delta < 7r$) could be due to the fact that the analytical solution does not take into account higher order terms that captures the proximity of the two bubble boundaries.

4.3. Two-bubble interaction: horizontal alignment

As mentioned by other authors [12,22], two bubbles rising side-by-side with $Re < 30$ will experience repulsion due to the

high pressure between the bubbles due to converging streamlines. Here it was found, as in [39], that two abreast bubbles rising in shear-thinning fluids also follow this rule; however, the thinning condition can considerably decrease the rate of separation between bubbles. In Fig. 14 the separation distance d^* is shown as a function of time t^* for the small ($0.4 < Re < 1.3$) and large ($4 < Re < 7.5$) bubbles and for several initial separation distances d_0^*. The experimental values are included as well as the numerical results. In this figure we can observe that the separation distance between bubbles increases with time for all the cases; nevertheless, it was found that the rate of separation decreases with the thinning property (there is hardly any separation in the $n = 0.55$ fluid). This behavior reveals that the low viscosity zone produced by the bubble pair weakens the repulsive force between the bubbles aligned horizontally and decreases the rate at which the two bubbles separate. Additionally, it can be seen that the slope of the curves slightly decrease as the initial separation is increased, revealing that the interaction is weaker for larger separations. The 2D numerical results showed the same general trend found in the experiments; however, the rate of separation was considerably higher. Other authors [58] have already reported important differences between 2D simulations and the experimental results. In our case, it seems that the disc-shaped bubbles overestimate the lift forces acting on each of their boundaries. A full 3D simulation would be needed to obtain a closer agreement with the experimental results.

Fig. 15 illustrates simulations of the lateral separation in Newtonian as well as in a shear-thinning fluid. Note that the bubbles separate from each other in both cases. In a general way, the experimental and numerical results obtained in this section suggest that the thinning behavior is not capable to attract two bubbles rising parallel in a fluid, unlike what has been observed in viscoelastic fluids [59,43]. Gheissary and van den Brule [60] observed an attractive behavior of two settling particles moving in a thinning fluid made with Carbopol. Nevertheless, it has to be pointed out that the fluids used by these authors had a viscosity above one thousand times that of water and presented a gel-like behavior. In this kind of fluids the shear-thinning behavior can be originated from the structure breakdown of the gel, as mentioned by the authors, giving place to a different behavior during the interaction of two bodies.

We calculated the instantaneous drag of the two bubbles rising side-by-side and compare it with the single bubble value for the case of the $n = 0.85$ fluid. The drag value of each bubble

small bubbles

large bubbles
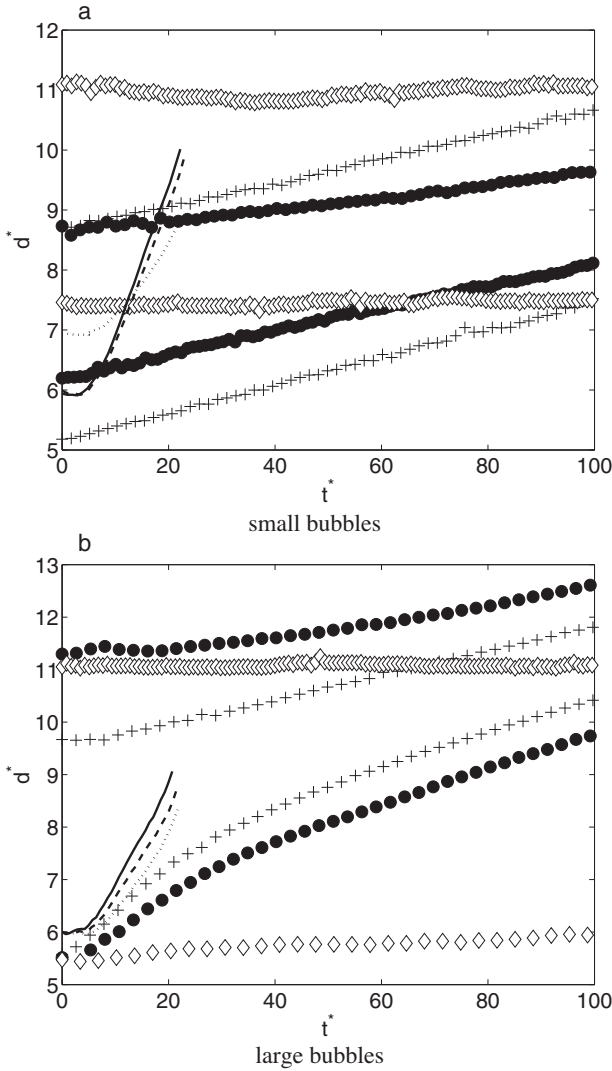
Fig. 14. Dimensionless distance in terms of the dimensionless time of two bubbles released side-by-side. (a) $d_b = 2.1$, $0.4 < Re < 1.3$; (b) $d_b = 3.6$, $4.0 < Re < 7.5$. Experimental results: (+) Newtonian fluid, (●) $n = 0.85$ fluid, (◇) $n = 0.55$ fluid. Numerical results: (—) Newtonian fluid, (– –) $n = 0.85$ fluid, (. . .) $n = 0.55$ fluid.
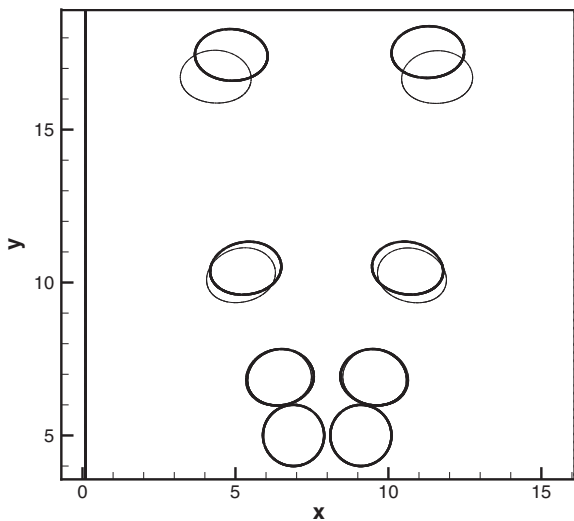
Fig. 15. Bubbles pair released side-by-side in the thinning $n = 0.55$ fluid (thick lines) and its Newtonian (thin lines) counterpart. The bubbles positions in both fluids were taken at the same time. Initial separation distance: $\delta = 2.2r$, $Re \sim 10$.
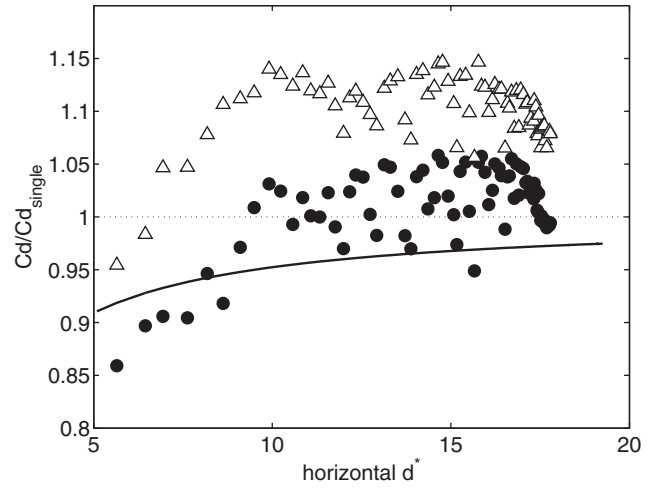
Fig. 16. Drag ratio Cd/Cd_{single} in terms of the horizontal distance d^* for two off-line bubbles released in the $n = 0.85$ fluid [22]. (●) left bubble, (△) right bubble, (−) $Cd/Cd_{single} = (1 + [1/2d^*])^{-1}$, $d_b = 3.7$ mm, $Re \approx 3.5$.

is equal to:

$$Cd = \frac{4d_b g}{3|\mathbf{v}|^2}\cos\beta = \frac{4d_b g V_z}{3|\mathbf{v}|^2|\mathbf{v}|} \tag{16}$$

where $|\mathbf{v}|$ is the net velocity, β the angle formed between the vertical axis and the vector $\mathbf{v}$ and V_z the vertical component of the velocity vector. The drag ratio Cd/Cd_{single} for each bubble is then obtained from the following expression:

$$\frac{Cd}{Cd_{single}} = \frac{V_z|\mathbf{v}|_{single}{}^3}{V_{z\,single}|\mathbf{v}|^3} = \frac{V_z V_{z\,single}{}^2}{|\mathbf{v}|^3} \tag{17}$$

The drag ratios for the left (the one formed at the central capillary) and right bubbles as a function of the horizontal distance d^* between bubble centers are shown in Fig. 16. The analytical expression found by Legendre et al. [22] for two spherical bubbles rising side-side in Newtonian fluids for the limiting case of $d^* \gg 1$ and $d^* Re \ll 1$ is also shown. It can be seen that the drag ratio decreases as the bubbles became closer. This agrees with the general trend found in viscous dominated flows, where the liquid encounters less resistance in moving around the two bodies rather than passing in the gap between them. The pair will then move as a single body. As the separation distance is increased, the drag value tends to the single bubble one. The differences in the values between the left and right bubbles are due to the proximity of the wall and the appearance of a slight differences in the vertical position between bubbles. The fact that the experimental values for the $n = 0.85$ fluid are close to the analytical expression of [22] indicates that in the limit of $d^* \gg 1$ the effect of the thinning behavior is irrelevant and only contributes to the value of the Re number at which the bubbles move. The results presented here are also in qualitative agreement with the behavior found by [31] for the case of rigid particles fixed in the space in an horizontal alignment.

We should point out that the role of the lateral movement experienced by two off-line bubbles, described in this section, on the formation of clusters in bubbly flows is not as clear as the in-line alignment where, as we saw in Section 4.2, two bubbles may or may not cluster depending on the inertia and deformability of the bubbles. Intuitively speaking, although a lateral repulsion between bubbles at low Re will give place to a higher homogeneity in the bubble spatial distribution on the horizontal plane, this effects will be secondary due to bubble attraction and pairing in the vertical plane and with angles $>40°$. This issue will be discussed further in the next section.

a

bubble position

b

dimensionless distance between bubbles as a function of time
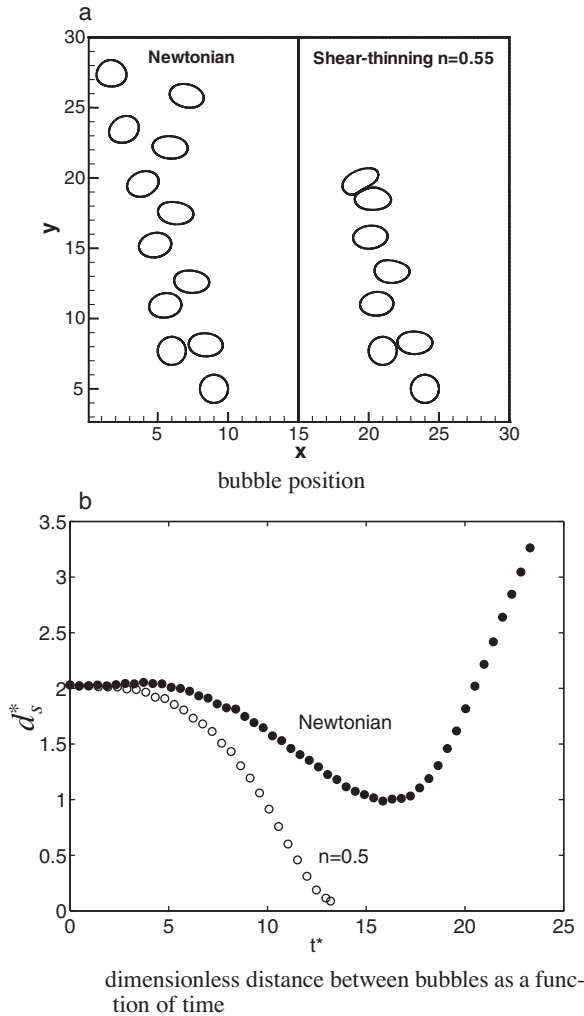
Fig. 17. Bubbles position and dimensionless separation distance for the $n = 0.55$ fluid and its Newtonian counterpart. The initial separation distance between bubble centers was $\delta = 4r$, the initial angle was $42°$, $Re \sim 10$.

4.4. Two-bubble interaction: varying the angle of approach

In this section we used the ALE code to gain some insight of the hydrodynamic interaction of a bubble pair which is not aligned horizontally nor vertically. For the experiments, although the production of bubbles to be aligned at an arbitrary angle (and preserving the same separation distance) is doable (consider, for example, a staggered initial arrangement); the necessary work to manipulate and change one arrangement for another could be rather arduous; hence, the use of simulations to predict the different behaviors is well justified. The case of the thinning fluid with $n = 0.55$ and its Newtonian counterpart is shown in Fig. 17a, where the initial separation between bubbles centers was $4r$ and the initial angle was $42°$. The variation of the dimensionless distance between bubbles is plotted against the dimensionless time in Fig. 17b. It can be seen that in the Newtonian fluid the bubbles approach each other but they do not make contact and eventually separate. On the other hand, in the thinning fluid the trailing bubble catches up with the leading one and makes contact with it. After this drafting and kissing process the bubbles do not separate, the so-called tumbling motion is not observed. This behavior indicates that the bubbles are "forced" to stay in a low viscosity region, produced by a high shear rate zone, rather than separate from each other (the same trend was seen experimentally with the in-line bubbles during the

non-tumbling stage). When the two interfaces come too close to each other (about $0.03r$), the local resolution becomes insufficient and the code eventually fails to converge. That was where the simulations in the thinning fluid ended.

To explore the effect of the degree of shear-thinning, we also carried out simulations with the $n = 0.85$ and 0.76 fluids, corresponding to the other experimental fluids used here and in [33]. The results are shown in Fig. 18 for three initial angles θ_0: $42°$, $61°$ and $76°$ with respect to the horizontal and for the same initial distance of $4r$. The Eo and Re numbers indicated in this figure were selected from the single bubble experiments in order to compare the simulations at a fixed value of Eo or Re. First we observed that for the Newtonian case, the bubbles separate after contact (data not shown). For this case we tested initial angles up to $88°$. In the shear-thinning fluids, the behavior at initial angle $\theta_0 \geq 61°$ (Fig. 18c–f) is more or less the same as for bubbles in tandem (see Fig. 9). That is, the two bubbles will form a doublet if $Mo \gtrsim 10^{-3}$ and will separate otherwise. For $\theta_0 = 42°$, the greater horizontal separation weakens the interaction between the bubbles such that doublet formation is achieved only for the most shear-thinning fluid in Fig. 18b. The $n = 0.55$ fluid in Fig. 18a has a $Mo = 2 \times 10^{-3}$ but anyway experience separation. For the other cases in Fig. 18a and b, there is an initial attraction between the two bubbles, but they eventually drift apart. The decrease of d^* in the $n = 0.55$ fluid (Fig. 18a) at $t^* = 20$ is due to the proximity of the wall.

In order to explain more in detail the results observed in Fig. 18, we compute the viscosity profile around a single bubble for the $n = 0.55$ and 0.85 fluids having the same Eötvös number ($Eo = 3$). The results shown in Fig. 19 are similar to the ones obtained by [53] for similar Re numbers ($Re \sim 10$). The maximum viscosity values agree well with the values given by the rheological data fitted with the Carreau model. We analyzed these viscosity profiles in two different ways: first, we introduced a definition of the viscosity gradient by computing the difference between the viscosity value on the bubble surface (η_{min}) and the viscosity value (η) located at two bubble diameters form the bubble surface. The curves of such viscosity gradient as a function of the angle formed with the horizontal plane is shown in Fig. 20a. Then, we compute the η/η_{min} ratio for different distances from the bubble surface at a fixed angle. The results for an angle of $20°$ are shown in Fig. 20b.

In Fig. 20a we can see that the viscosity gradient is not homogeneous around the bubble due to the presence of the bubble wake, which extends the region of non-zero shear rate and hence increase the region of viscosity recovery. On the other hand, near the horizontal plane, the decay of the shear rate occurs in a smaller region; therefore, the values of the viscosity gradient are larger. For the cases shown in Fig. 20a the maximum viscosity gradient occurs at an angle of $20°$ in both fluids; however, the viscosity gradient found in the $n = 0.55$ at this angle is 5 times larger than the one found in the $n = 0.85$ fluid. The fact that the higher values of the viscosity gradient lie near the horizontal plane could explain why the fluids with higher thinning behavior can promote bubble clustering at lower angles, as we saw in Fig. 18. In this sense we think that the viscosity gradients produce a stress distribution that is different from that of a Newtonian fluid; such stress gradients will not work as a net driving force but will reduce the repulsive force created by the bubble vortices, causing the trailing bubble to remain trapped by the wake of the leading one.

In Fig. 20b we can see how the viscosity ratio η/η_{min} increases with the distance from the bubble surface. The difference between the $n = 0.55$ (clustering condition) and 0.85 (free bubble condition) fluids is clear: in the case of the most thinning fluid the viscosity ratio reaches a value of 27, while in the other fluid reaches only a value of 3 at the same d_s^*. The viscosity gradient of the $n = 0.55$ fluid depicted in Fig. 20 acts as a viscosity "hole" which prevents another bubble to escape from the low viscosity region.
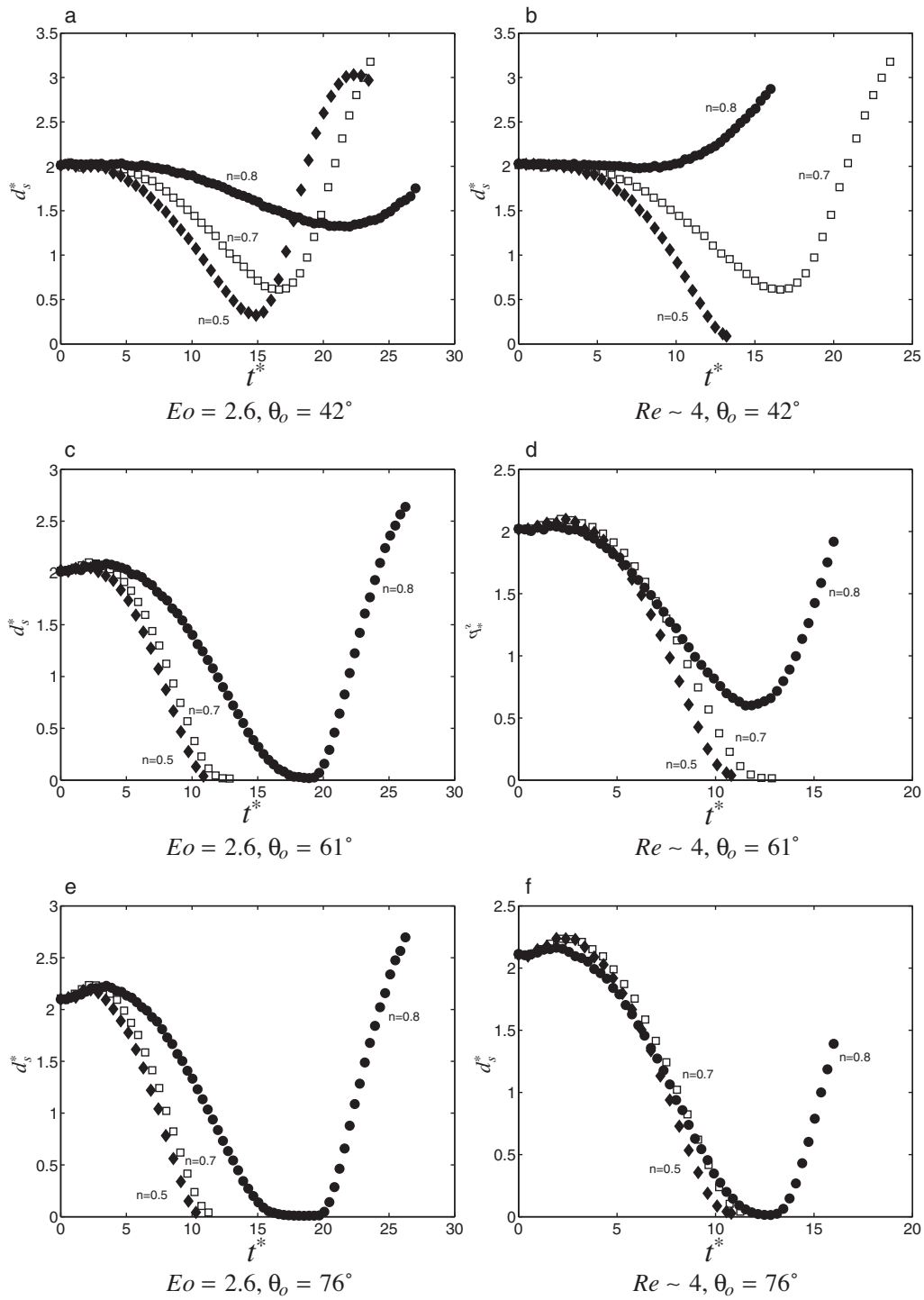
Fig. 18. Dimensionless distances d_s^* between bubble boundaries as a function of the time t^* for several thinning conditions and initial angles. ($\bullet$) $n = 0.85$, ($\square$) $n = 0.76$, ($\blacklozenge$) $n = 0.55$; initial distance, $\delta = 4r$. For the left column $Eo = 2.6$ is fixed, for the right column $Re \sim 4$ is fixed. The experimental Mo number for the $n = 0.55$ fluid is 2×10^{-3} and for the other fluids is around 7×10^{-4}.

To compare the viscosity profile obtained for a single bubble with the one obtained for a bubble pair, we compute the viscosity of two bubbles in contact rising in the $n = 0.55$ fluid. The results are shown in Fig. 21. In this case we can see that the region of the lowest viscosity value ($\sim 0.05 \, \text{Pa} \cdot \text{s}$) comprises a larger area than the one occupied in the single bubble case. We may think then that the increase of the cluster size will increase the region of the lowest viscosity value but at the same time decrease the viscosity gradients. Note also that in the rear part of the bubble pair a region

of high viscosity start to form due to the appearance of a toroidal vortex, in agreement with [53].

From all these observations we can propose three mechanisms for cluster formation in shear-thinning fluids: (i) The viscosity gradients that appear in the wake of a bubble ascending in a thinning fluid reduce the repulsive force from the bubble vortices. This makes possible for a bubble to be caught in the wake of another bubble; if the thinning behavior increases, the critical angle of inversion of the lift force (from repulsion to attraction) is decreased, leading
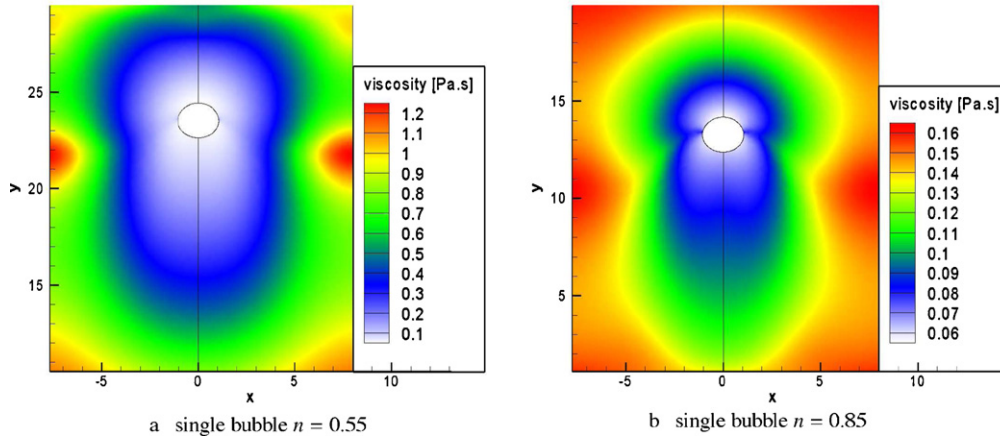
Fig. 19. Viscosity contours around a single bubble immersed in the $n = 0.55$ and 0.85 fluids. The viscosity was estimated when the bubbles achieved a steady velocity, $t^* = 7.6$, $Eo = 3$. To avoid high viscosity values at low shear rates, an upper limit to the viscosity was introduced fitting the rheological data with the Carreau model $\eta = \eta_\infty + (\eta_0 - \eta_\infty)(1 + [\lambda\dot{\gamma}]^2)^{(n-1)/2}$, where η_0 is the zero-shear viscosity value, η_∞ the viscosity at high shear rates, λ a time constant and n the flow index.
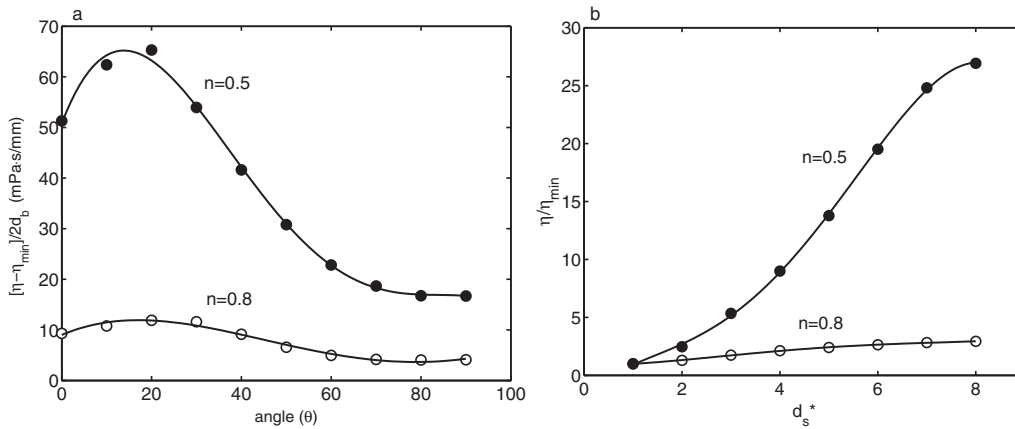
Fig. 20. (a) Values of the viscosity gradient as a function of the angle made with the horizontal plane for the bubbles presented in Fig. 19, $d^* = 5r$. (b) Viscosity ratio as a function of the dimensionless distance at a fixed angle of $20°$.
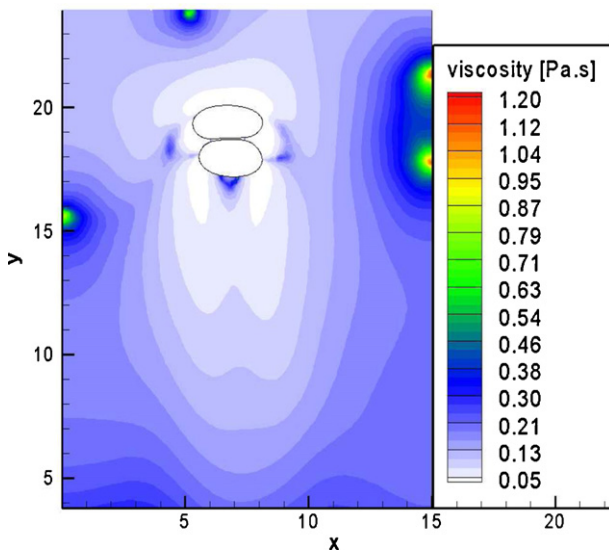

Fig. 21. Viscosity contours around a bubble pair immersed in the $n = 0.55$ fluid. The viscosity was estimated when the bubbles achieved a gap separation distance of $0.06r$, $Eo = 3$. The initial angle was $76°$. The Carreau model was again used as in Fig. 19.

to a more effective clustering; (ii) if the Morton number is higher than 10^{-3}, the bubbles do not tumble after contact, a doublet is then formed; (iii) once two bubbles form a pair, they create a wake with lower viscosity which attracts more bubbles, leading to the formation of bubble clusters; however, the increase of the cluster size will decrease the viscosity gradient (so attaining a Newtonian-like behavior) and the growth of the clusters will then stop. We need to point out here that the cluster deformability (imagining the cluster as one big bubble) must also play an important role in the increment of its size. As mentioned by Manga and Stone [16,17], the increase of the deformability of the bubble surface leads to the formation of streamlines that propitiates the alignment and contact of two separate bubbles. The velocity field formed around a cluster can also trap additional bubbles that contribute to its growth.

The thinning property reduces the hydrodynamic repulsive force that results from the converging streamlines. Let us consider shear stress in a Newtonian fluid: $\tau = -\eta\dot{\gamma}$. This relation can be interpreted as the momentum transfer from high to low regions of shear, that is, the momentum per unit area and time is proportional to the negative of the velocity gradient [61]. Hence, the momentum flux per unit time and volume, P, can be calculated as the gradient of the shear stress. Considering now the power law model $\tau = -k\dot{\gamma}^n$ we can calculate P as:

$$P = -\frac{\partial}{\partial y}(\eta\dot{\gamma}) \tag{18}$$
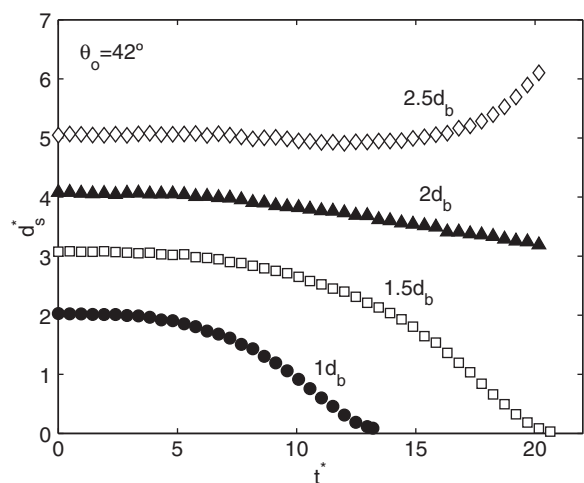
Fig. 22. Dimensionless distance between bubble boundaries as a function of the dimensionless time (t^*) for the $n = 0.5$ fluid and several separation distances. (●) $d_s^* = 2$, (□) $d_s^* = 3$, (▲) $d_s^* = 4$, (◇) $d_s^* = 5$, initial angle: $42°$.

where $\eta = k\dot{\gamma}^{n-1}$. Therefore,

$$P = -\eta(n-1)\dot{\gamma}' - \eta\dot{\gamma}' \tag{19}$$

where $\dot{\gamma}' = \partial\dot{\gamma}/\partial y$. Comparing this expression with the Newtonian one, we have:

$$\frac{P}{P_N} = \frac{\eta}{\eta_N} + (n-1)\frac{\eta}{\eta_N} \tag{20}$$

In the case of a Newtonian fluid ($n = 1$), $P/P_N = 1$, as expected. However, if the fluid is shear-thinning, the ratio P/P_N decreases with n, that is, the momentum transport decreases as the fluid becomes more shear thinning. Hence, the viscosity gradients that appear around the leading bubble will reduce momentum transfer which, in turn, will tend to keep the trailing bubble trapped behind the leading one.

We have seen that for all the fluids studied here, including the Newtonian one, the trailing bubbles located within an angle of $40°$ with respect to the horizontal do not contact the leading one. On the contrary, bubbles located outside this region, that is, closer to the vertical axis, experience an attractive force that leads to the contact between bubbles. This behavior is the opposite to that observed for high Re flows where, according to [19,20,62], two bubbles positioned with an angle within the $35–54°$ experience attraction, while with an angle above $35–54°$, near the vertical axis, experience repulsion. The general description of the bubble motion in terms of the angle of approach in this work is in agreement with other experimental work [39] for the case of the thinning fluids.

Finally, aside from the shear-thinning behavior and angle of alignment, we can expect the bubble-bubble interaction to be also dependent on the separation distance between bubbles. This effect is shown in Fig. 22 for a fixed flow index value and initial angle ($n = 0.55$ and $42°$). We can see that when the distance between bubbles surpasses two bubble diameters, the trailing bubble is no longer attracted by the leading one; in fact, they become nearly horizontally aligned and start increasing their separation distance. The same trend was seen with the other thinning fluids. These results suggest that in dilute bubbly flows, bubble clusters will not be formed due to the distance between them. Nevertheless this condition is difficult to achieve experimentally [33].

5. Conclusions

The interaction of two bubbles rising in shear-thinning inelastic fluids ($0.55 < n < 1.0$) was studied by following the bubbles trajec-

tories with a movable camera. The bubbles were released by a pair of capillaries in a vertical and a horizontal alignment. The experiments were complemented by numerical simulations conducted with the arbitrary Lagrangian–Eulerian technique. In this way, a full range of angles of approach between the bubbles was studied. These were the relevant observations:

1. Before contact, the bubble trajectories followed the general behavior found in Newtonian flows for $Re < 30$: a divergent path or repulsion between bubbles if the angle of approach lay within $40°$ from the horizontal, and a convergent path or attraction otherwise.
2. In shear-thinning fluids, the wake formed behind a leading bubble attracts the trailing bubble. This attractive motion was increased with the amount of shear-thinning (decreasing the flow index). This effect was nevertheless hindered by the inertial effects.
3. The numerical simulations suggested that the angle of inversion of the lift force between two rising bubbles can decrease due to the high viscosity gradient formed near the horizontal plane of the bubbles when rising in a thinning fluid.
4. After the drafting and kissing processes, bubbles rising in thinning fluids tend to stay together (not-tumbling) depending on the inertia and deformability of the single bubble. This proved to be an important difference between Newtonian and non-Newtonian flows. Furthermore, the bubbles forming pairs showed an oscillatory motion due to the reduced viscosity being formed by the leading bubble and the subsequent acceleration of the trailing one. In Newtonian flows, only the bubbles rising at $Re < 1$ formed pairs.

This study of the interaction of a bubble pair is a significant step toward understanding multiphase flow systems. In particular, we saw that two bubbles rising in a thinning fluid have a different behavior than the one observed with the single ones; the mechanism of doublet formation provides a better understanding of the clustering mechanism observed in shear-thinning inelastic bubbly flows [33].

References

[1] Y.T. Shah, B.G. Kelkar, S.P. Godbole, W.-D. Deckwer, Design parameters estimation for bubble column reactors, AIChE J. 28 (1982) 353.
[2] P.M. Kilonzo, A. Margaritis, The effects of non-Newtonian fermentation broth viscosity and small bubble segregation on oxygen mass transfer in gas-lift bioreactors: a critical review, Biochem. Eng. J. 17 (2004) 27.
[3] N. Kantarci, F. Borak, K.O. Ulgen, Bubble column reactors, Process Biochem. 40 (2005) 2263.
[4] R.R. Lessard, S.A. Zieminski, Bubble coalescence and gas transfer in aqueous electrolytic solutions, Ind. Eng. Chem. Fundam. 10 (1971) 260.
[5] K.L. Tse, T. Martin, C.M. McFarlane, A.W. Nienow, Small bubble formation via a coalescence dependent break-up mechanism, Chem. Eng. Sci. 58 (2003) 275.
[6] Y. Liao, D. Lucas, A literature review on mechanisms and models for the coalescence process of fluid particles, Chem. Eng. Sci. 65 (2010) 2851.
[7] J.R. Crabtree, J. Bridgwater, Bubble coalescence in viscous liquids, Chem. Eng. Sci. 26 (1971) 839.
[8] J. Katz, C. Meneveau, Wake-induced relative motion of bubbles rising in line, Int. J. Multiphase Flow 22 (1996) 239.
[9] T. Sanada, A. Sato, M. Shirota, M. Watanabe, Motion and coalescence of a pair of bubbles rising side by side, Chem. Eng. Sci. 64 (2009) 2659.

[10] M. Stimson, G.B. Jeffery, The motion of two spheres in a viscous fluid, Proc. Roy. Soc. A111 (1926) 110.
[11] J. Happel, H. Brenner, Low Reynolds Number Hydrodynamics, Kluwer Academic Publishers, 1991.
[12] J. Happel, R. Pfeffer, The motion of two spheres following each other in a viscous fluid, AIChE J. 6 (1960) 129.
[13] D. Bhaga, M.E. Weber, In-line interaction of a pair of bubbles in a viscous liquid, Chem. Eng. Sci. 35 (1980) 2467.
[14] S. Narayanan, L.H.J. Goossens, N.W.F. Kossen, Coalescence of two bubbles rising in line at low Reynolds numbers, Chem. Eng. Sci. 29 (1974) 2071.
[15] J. Zhang, L.-S. Fan, On the rise velocity of an interactive bubble in liquids, Chem. Eng. J. 92 (2003) 169.
[16] M. Manga, H.A. Stone, Buoyancy-driven interactions between two deformable viscous drops, J. Fluid Mech. 256 (1993) 647.
[17] M. Manga, H.A. Stone, Collective hydrodynamics of deformable drops and bubbles in dilute low Reynolds number suspensions, J. Fluid Mech. 300 (1995) 231.
[18] L. van Wijngaarden, Hydrodynamic interaction between gas bubbles in liquid, J. Fluid Mech. 77 (1976) 27.
[19] A. Biesheuvel, L. van Wijngaarden, The motion of pairs of gas bubbles in a perfect liquid, J. Eng. Math. 16 (1982) 349.
[20] J.B.W. Kok, Dynamics of a pair of gas bubbles moving through liquid. Part I. Theory, Eur. J. Mech. B/Fluids 12 (1993) 515.
[21] P. Vasseur, R.G. Cox, The lateral migration of spherical particles sedimenting in a stagnant bounded fluid, J. Fluid Mech. 80 (1977) 561.
[22] D. Legendre, J. Magnaudet, G. Mougin, Hydrodynamic interactions between two spherical bubbles rising side by side in a viscous liquid, J. Fluid Mech. 497 (2003) 133.
[23] H. Yuan, A. Prosperetti, On the in-line motion of two spherical bubbles in a viscous fluid, J. Fluid Mech. 278 (1994) 325.
[24] M. Watanabe, T. Sanada, In-line motion of a pair of bubbles in a viscous liquid, JSME Int. J., Ser. B 49 (2006) 410.
[25] Y. Hallez, D. Legendre, Interaction between two spherical bubbles rising in a viscous liquid, J. Fluid Mech., submitted for publication.
[26] I. Kim, S. Elghobashi, W.A. Sirignano, Three-dimensional flow over two spheres placed side by side, J. Fluid Mech. 246 (1993) 465.
[27] J.B.W. Kok, Dynamics of a pair of gas bubbles moving through liquid. Part II. Experiment, Eur. J. Mech. B/Fluids 12 (1993) 541.
[28] K.O.L.F. Jayaweera, B.J. Mason, G.W. Slack, The behavior of cluster of spheres falling in a viscous fluid, J. Fluid Mech. 20 (1964) 121.
[29] C.E. Brennen, Cambridge University Press, in: Fundamentals of Multiphase Flow, 2005.
[30] M.C. Ruzicka, On bubbles rising in line, Int. J. Multiphase Flow 26 (2000) 1141.
[31] S.-C. Liang, T. Hong, L.-S. Fan, Effects of particle arrangements on the drag force of a particle in the intermediate flow regime, Int. J. Multiphase Flow 22 (1996) 285.
[32] A. Cartellier, L. Timkin, N. Rivière, New structures of Poiseuille bubbly flows due to clustering, Proc. ASME-FEDSM' 97, paper 3528, Vancouver, June 22–26, 1997.
[33] J. Rodrigo VéJ. Rodrigo Vélez-Cordero, R. Zenit, Bubble cluster formation in shear-thinning inelastic bubbly columns, J. Non-Newtonian Fluid Mech. 166 (2010) 32–41.
[34] R. Zenit, D.L. Koch, A.S. Sangani, Measurements of the average properties of a suspension of bubbles rising in a vertical channel, J. Fluid Mech. 429 (2001) 307.
[35] H.Z. Li, Y. Mouline, D. Funfschilling, P. Marchal, L. Choplin, N. Midoux, Evidence for in-line bubble interactions in non-Newtonian fluids, Chem. Eng. Sci. 53 (1998) 2219.
[36] S. Radl, G. Tryggvason, J.G. Khinast, Flow mass transfer of fully resolved bubble in non-Newtonian fluids, AIChE J. 53 (2007) 1861.
[37] H.Z. Li, Y. Mouline, L. Choplin, N. Midoux, Rheological simulation of in-line bubble interactions, AIChE J. 43 (1997) 265.
[38] R.G. Sousa, A.M.F.R. Pinto, J.B.L.M. Campos, Interaction between Taylor bubbles rising in stagnant non-Newtonian fluids, Int. J. Multiphase Flow 33 (2007) 970.
[39] F. Wenyuan, M. Youguang, L. Xiaolei, L. Huaizhi, Study on the flow field around two parallel moving bubbles and interaction between bubbles rising in CMC solutions by PIV, Chin. J. Chem. Eng. 17 (2009) 904.
[40] J.P. Singh, M.M. Denn, Interacting two-dimensional bubbles and droplets in a yield-stress fluid, Phys. Fluids 20 (2008) 040901.
[41] J. Tsamopoulos, Y. Dimakopoulos, N. Chatzidai, G. Karapetsas, M. Pavlidis, Steady bubble rise and deformation in Newtonian and viscoplastic fluids and conditions for bubble entrapment, J. Fluid Mech. 601 (2008) 123.
[42] F. Calderas, A. Sanchez-Solis, A. Maciel, O. Manero, The transient flow of the PET–PEN–montmorillonite clay nanocomposite, Macromol. Symp. 283–284 (2009) 354.
[43] H.H. Hu, N.A. Patankar, M.Y. Zhu, Direct numerical simulations of fluid-solid systems using the arbitrary Lagrangian–Eulerian technique, J. Comput. Phys. 169 (2001) 427.
[44] P. Yue, J.J. Feng, C.A. Bertelo, H.H. Hu, An arbitrary Lagrangian–Eulerian method for simulating bubble growth in polymer foaming, J. Comput. Phys. 226 (2007) 2229.
[45] A. Prosperetti, G. Tryggvason, Computational Methods for Multiphase Flow, Cambridge University Press, 2009.
[46] S.M. Bhavaraju, R.A. Mashelkar, H.W. Blanch, Bubble motion and mass transfer in non-newtonian fluids: Part II. Swarm of bubbles in a power law fluid, AIChE J. 24 (1978) 1070.
[47] T. Hirose, M. Moo-Young, Bubble drag and mass transfer in non-Newtonian fluids: creeping flow with power-law fluids, Can. J. Chem. Eng. 47 (1969) 265.
[48] D. Rodrigue, D. De Kee, C.F. Chan Man Fong, A note on the drag coefficient of a single gas bubble in a power-law fluid, Can. J. Chem. Eng. 77 (1999) 766.
[49] N.W. Haque, K.D.P. Nigam, K. Viswanathan, J.B. Joshi, Studies on bubble rise velocity in bubble columns employing non-Newtonian solutions, Chem. Eng. Commun. 73 (1988) 31.
[50] D. Chehata, Estudio de la Discontinuidad en la Velocidad de Ascenso de una Burbuja en un Fluido no Newtoniano, M.Sc. thesis, Universidad Nacional Autónoma de México, 2004.
[51] S.D. Dhole, R.P. Chhabra, V. Eswaran, Drag of a spherical bubble rising in power law fluids at intermediate reynolds numbers, Ind. Eng. Chem. Res. 46 (2007) 939.
[52] N. Kishore, R.P. Chhabra, V. Eswaran, Drag on ensembles of fluid spheres translating in a power-law liquid at moderate Reynolds numbers, Chem. Eng. J. 139 (2008) 224.
[53] L. Zhang, C. Yang, Z.-S. Mao, Numerical simulation of a bubble rising in shear-thinning fluids, J. Non-Newtonian Fluid Mech. 165 (2010) 555.
[54] R. Clift, J.R. Grace, M.E. Weber, Bubbles, Drops and Particles, Academic Press, NY, 1978.
[55] L.M. Hocking, The behavior of clusters of spheres falling in a viscous fluid, J. Fluid Mech. 20 (1964) 129.
[56] E. Rushton, G.A. Davies, Slow unsteady settling of two fluid spheres along their line of centers, Appl. Sci. Res. 28 (1973) 37.
[57] F.A. Morrison, Breakup of a bubble chain, Chem. Eng. Sci. 28 (1973) 1115.
[58] K. Ekambara, M.T. Dhotre, J.B. Joshi, CFD simulations of bubble column reactors: 1D, 2D and 3D approach, Chem. Eng. Sci. 60 (2005) 6733.
[59] D.D. Joseph, Y.J. Liu, M. Poletto, J. Feng, Aggregation and dispersion of spheres falling in viscoelastic liquids, J. Non-Newtonian Fluid Mech. 54 (1994) 45.
[60] G. Gheissary, B.H.A.A. van den Brule, Unexpected phenomena observed in particle settling in non-Newtonian media, J. Non-Newtonian Fluid Mech. 67 (1996) 1.
[61] R.B. Bird, W.E. Stewart, E.N. Lightfoot, Transport Phenomena, John Wiley & Sons, Inc., New York, 1998.
[62] P.D.M. Spelt, A.S. Sangani, Properties averaged equations for flows of bubbly liquids, Appl. Sci. Res. 58 (1998) 337.